Published July , 1978

LASER MICROBEAM STUDY OF A ROTARY MOTOR IN TERMITE FLAGELLATES

Evidence That the Axostyle Complex Generates Torque

SIDNEY L. TAMM

From the Laboratory of Molecular Biology, University of Wisconsin, Madison, Wisconsin 53706

ABSTRACT

A rotary motor in a termite flagellate continually turns the anterior part of the cell (head) in a clockwise direction. Previous descriptive observations implicated the noncontractile axostyle, which runs through the cell like a driveshaft, in the motile mechanism. This study demonstrates directly that the axostyle complex generates torque, and describes several of its dynamic properties.

By laser microbeam irradiation, the axostyle is broken into an anterior segment attached to the cell's head, and a posterior segment which projects caudally as a thin spike, or axostylar projection. Before lasing, both head and axostylar projection rotate at the same speed. After breaking the axostyle, the rotation velocity of the head decreases, depending on the length of the anterior segment. Head speed is not a linear function of axostyle length, however. In contrast, the rotation velocity of the axostylar projection always increases about 1.5 times after lasing, regardless of the length of the posterior segment. Turning the head is thus a load on the axostylar rotary motor, but the speed of the posterior segment represents the free-running motor. A third, middle segment of the axostyle, not connected to the head or axostylar projection, can also rotate independently.

No ultrastructural differences were found along the length of the axostyle complex, except at the very anterior end; length-velocity data suggest that this region may not be able to generate torque. An electric model of the axostylar rotary motor is presented to help understand the length-velocity data.

KEY WORDS rotary motor · axostyle · laser microbeam · termite flagellate · chorion

Taking a machine apart helps to understand how it works. Here this approach is used to investigate a remarkable type of biological motor in eukaryotic cells. Instead of taking the motor apart, however, it is broken apart by laser irradiation.

The motor is responsible for a unique kind of cell motility in flagellate protozoans from termites (15–17). The anterior end or head of the cell continually rotates in the same direction relative to the cell body, at speeds up to 0.7 rotation/s. Rotation includes the plasma membrane as well as the cytoplasm. Since both thin sectioning and freeze-fracture[1] show that the plasma membrane is continuous across the "shear zone," this system provides direct, visible evidence for the fluid nature of cell membranes.

Previous work pointed to the noncontractile

[1] Tamm, S. L. Membrane movements and fluidity during rotational motility of termite flagellates. A freeze-fracture study. Manuscript submitted for publication.

Published July , 1978

axostyle complex as the rotary mechanism (15, 16). However, direct evidence that the axostyle complex generates torque was lacking.

In this study a laser microbeam is used to break the axostyle at various sites along its length, and the effects on rotational motility are determined. The results provide direct evidence that the axostyle complex is the rotary motor and they reveal several of its dynamic properties. A preliminary account of some of these results has been presented elsewhere (15).

MATERIALS AND METHODS

Organism

The protozoan used in this study is an unnamed devescovinid flagellate from the hindgut of *Cryptotermes cavifrons*. The cell resembles *Caduceia kofoidi* (8).

Wood containing *C. cavifrons* was collected in southern Florida and stored in the laboratory. Termites were kept in the original wood until used for experiments.

Preparation and Experimental Conditions

Hindguts from several termites were teased apart on a microscope slide in a drop of buffered saline containing acridine red (BARS solution). In most experiments, BARS solution consisted of 0.57% NaCl, 0.005 M $NaPO_4$ buffer, and 0.05% acridine red (pH 6.7). The preparation was immediately sealed off from the air with a Vaseline-ringed cover slip.

Devescovinids in BARS preparations exhibit vigorous rotational motility for at least several hours, similar to preparations made without acridine red.

Rotation velocity remains remarkably constant with time in vitro. This is true both for non-irradiated cells, which were followed for up to 3 h after being placed in BARS solution, and for lased cells, where rotation speed of the head was measured periodically for more than 1 h after lasing in some cases (cf. Fig. 5).

Laser experiments were usually performed within 40–100 min after making BARS slide preparations (~70 min on the average). By this time the cells had stopped swimming and had undergone a characteristic in vitro shape change which caused the distal part of the axostyle to project caudally from the cell body (see Results). Both the "head" of the cell and the caudal projection of the axostyle rotated clockwise (as viewed from anterior) at the same speed, while the cell body remained stationary.

Laser Apparatus

A pulsed argon ion laser (TRW model 71B, Quantrad Corp., El Segundo, Calif.) was focused through a Zeiss universal microscope to a 3–5 μm diameter beam, and aligned by conventional methods (4).

A cine camera (Locam, Redlake Corp., Photo Instrument Div., Santa Clara, Calif.) was used to record rotational velocities of lased cells in certain cases (Fig. 7).

Lasing

The axostyle is surrounded along most of its length by intracellular wood particles, which devescovinids (and other hindgut flagellates) digest. These wood particles become rapidly and intensely stained by acridine red.

To break the axostyle at a given site, an acridine red-stained wood particle lying close to the axostyle at this level (cf. Fig. 3 b) was irradiated for several seconds. The particle became swollen and spherical (Fig. 1 b); if it was not sufficiently close to the axostyle, no break resulted. In all experiments except one (Fig. 9), single breaks were made in the proximal part of the axostyle lying within the cell body, producing an anterior segment attached to the cell's head, and a posterior segment continuous with the caudal projection of the axostyle (Fig. 1 b).

Rotation Velocity Measurements

Rotation velocity was measured with a stopwatch as the time required for five consecutive rotations (t_5). Typically, three or four t_5 measurements were made for each velocity determination, and the average was used. Rotation speed of the axostyle before lasing was determined by measuring the rotation velocity of the head (which equals that of the axostylar projection). Only vigorous cells were used (0.4–0.7 rotations/s; average speed = 0.5 rotations/s). After lasing, rotation velocities of anterior and posterior segments were determined by measuring the rotation speeds of the head and axostylar projection, respectively. Rotation velocity was expressed as the relative change after lasing, i.e., $\frac{\text{velocity after lasing}}{\text{velocity before lasing}}$.

Axostyle Length Measurements

Axostyle lengths were measured directly on living cells with an ocular micrometer (1 U = 1.2 μm). Lengths before and after lasing were measured as shown in Fig. 1.

Lengths of anterior and posterior segments were expressed as fractions of the length of axostyle in the cell body before lasing. Relative lengths of anterior segments were calculated in two ways: $\frac{A_a}{A}$ and $\frac{A_a - A_b}{A - A_b}$ (cf. Fig. 1). The first method includes the bacteria-enclosed anteriormost part of the axostyle; however, several components of the axostyle complex are missing in this region (see Results). The latter method excludes this part of the axostyle from length-velocity plots (see Fig. 6 a vs. 6 b).

Relative lengths of posterior segments were calculated only as $\frac{A_p}{A - A_b}$, since rotation speed of the axostylar projection is independent of length (Fig. 8).

Published July , 1978

Electron Microscopy

The structure of anterior vs. posterior regions of the axostyle was determined in non-irradiated devescovinids fixed under conditions similar to those used in the laser experiments. Cells were kept in BARS slide preparations for about 70 min, but not lased. They were then fixed in paraformaldehyde-glutaraldehyde and processed as described previously (17). Sections were stained with uranyl and lead, and viewed in a Philips 300 electron microscope at 80 kV.

RESULTS

Structure of the Axostyle Complex

The axostyle itself is a straight rod, 80–120 μm long and about 2 μm in diameter, running centrally through the length of the cell. The main trunk of the axostyle begins at the base of the anteriorly situated nucleus. A helical Golgi apparatus is coiled around the posterior part of the nucleus and the very beginning of the axostyle (Figs. 1 and 2). Immediately behind the Golgi

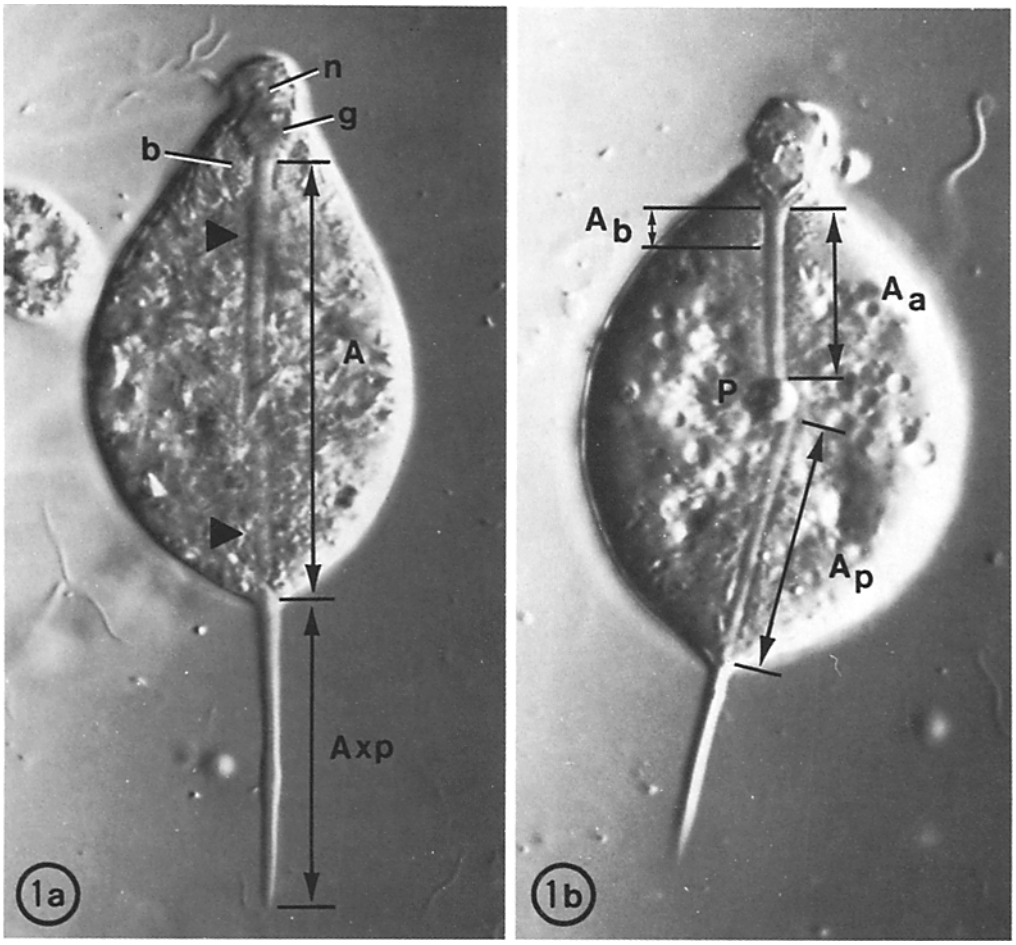

FIGURE 1 Devescovinids before (a) and after (b) laser-induced dissection of the axostyle. The proximal part of the axostyle lying within the cell body (*A* in Fig. 1 a) was broken at various levels by irradiating a nearby wood particle stained with acridine red. After lasing (b), an anterior segment (A_a) attached to the head of the cell, and a posterior segment (A_p) continuous with the axostylar projection (*Axp*) were produced. The lased wood particle swelled (*P*) and usually hid the broken ends of the axostyle; segment lengths were commonly measured to the apparent ends at the edges of the particle. In this cell, however, the end of the posterior segment is just visible at the lower edge of the particle. Note that axostyle lengths were measured from the base of the helical Golgi apparatus (*g*), and that the anteriormost 5–6 μm of the axostyle (A_b) is surrounded by a bowl-shaped group of intracellular bacteria (*b*; cf. Figs. 2 and 4 a).

Black triangles in Fig. 1 a point to approximate levels of sections through anterior (cf. Figs. 3 a and 4 b) and posterior (cf. Figs. 3 b and 4 c) regions of the axostyle complex. Zeiss Nomarski interference optics, electronic flash, Kodak high contrast copy film. (a) × 960. (b) × 1,100.

Published July , 1978

FIGURE 2 Longitudinal section through the anterior region of the axostyle complex. Arrows show termination of investing microfilaments (*mf*) in the region surrounded by bacteria (*b*). *mt*, microtubules; *n*, nucleus; *g*, Golgi apparatus; *ig*, inner girdle; *og*, outer girdle; *rb*, ectobiotic rod bacteria (see text). × 14,000.

Published July , 1978

apparatus is a bowl-shaped group of intracellular bacteria which surrounds the anteriormost 5–6 μm of the axostyle (Figs. 1, 2, and 4 a).

Freshly isolated devescovinids are cigar shaped with the entire length of the axostyle enclosed by body cytoplasm. In vitro, the flagellates become rounder anteriorly, leaving the distal part of the axostyle projecting caudally as a thin spike, closely surrounded by an extension of the cell membrane (Fig. 1). The length of the proximal part of the axostyle, i.e., within the cell body, usually measured ~60 μm.

The axostyle itself is a spiral sheet of ~400 microtubules which run parallel to the long axis of the rod (Figs. 2–4). Not all the microtubules begin at the base of the nucleus; some continue anteriorly along one side of the nucleus and overlap with another set (pelta microtubules) that runs under the membrane of the head.

A single layer of microfilaments, 50–70 Å in diameter, closely invests the microtubular spiral (Figs. 2–4). These filaments run at right angles to the long axis of the microtubules, and appear as a line of closely spaced dots on either side of the axostyle in longitudinal sections (Figs. 2 and 3).

The axostyle is also surrounded by a differen-

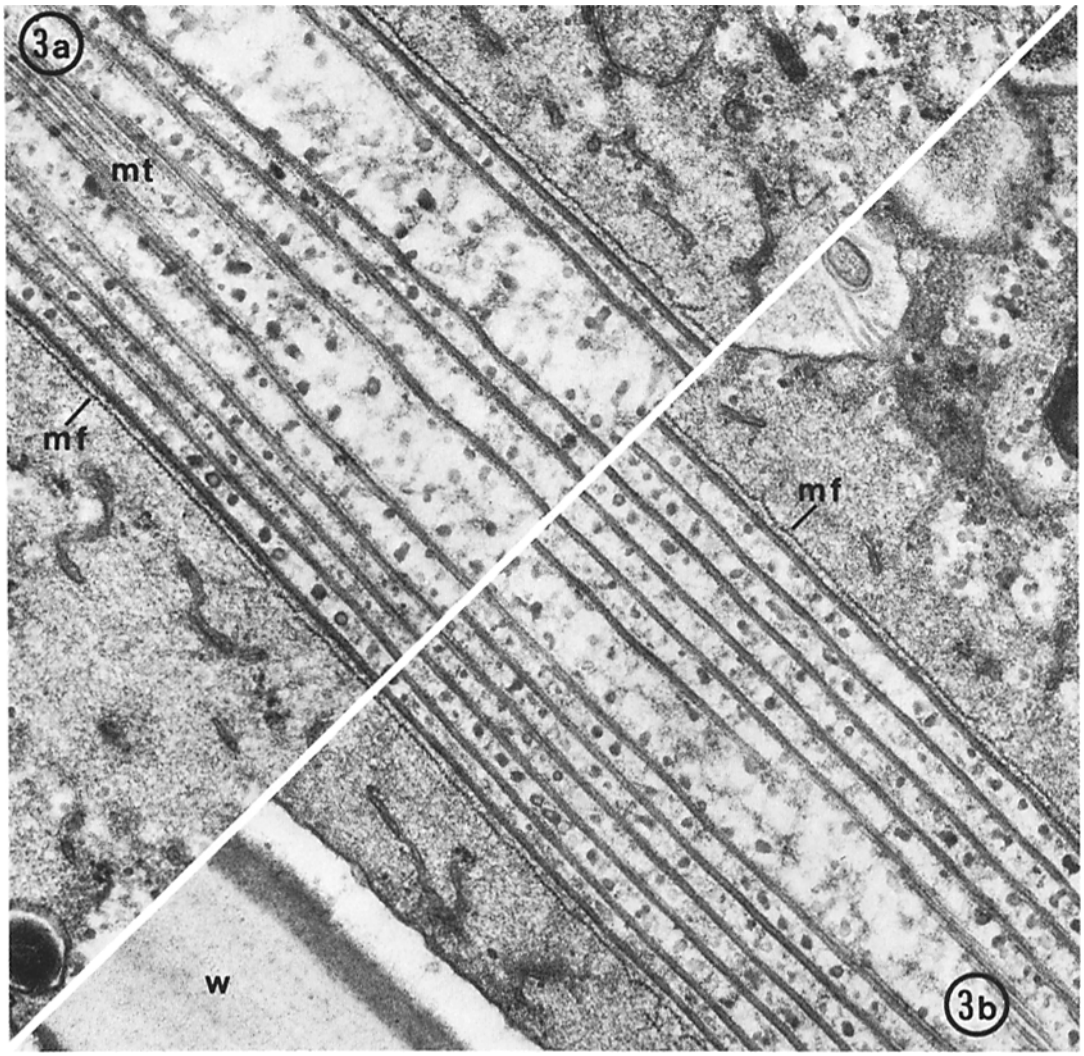

FIGURE 3 Longitudinal sections through anterior (a) and posterior (b) regions of the axostyle complex in the same cell, corresponding to the levels shown in Fig. 1 a. *mt*; microtubules; *mf*, microfilaments; *w*, wood particle close to axostyle, such as used for laser target (see text). × 43,700.

Published July , 1978

tiated girdle of cytoplasm. The girdle appears by light microscopy as a narrow, clear inner layer immediately adjacent to the rod itself, and a more irregular, granular outer layer. During rotation of the axostyle, the outer layer of the girdle remains stationary, but there are no visible markers for the inner girdle.

In the electron microscope the inner girdle consists of a fine, fibrillar-granular matrix in which a system of membranous sacs and tubules is dispersed (Figs. 2–4). The "granules" of the outer layer of the girdle are double membrane-bounded bodies of unknown nature, containing material which resembles the matrix of the inner girdle.

The microtubular rod, or axostyle proper, together with the surrounding microfilaments and girdle is called the axostyle complex.

Several components of the axostyle complex are missing in the region surrounded by the bowl-shaped group of bacteria at the anterior end (Figs. 2 and 4 a). This part of the axostyle is largely devoid of the microfilaments. Although the fibrillar-granular matrix of the inner girdle is present, the membranous elements are absent. The outer layer of the girdle, i.e., the double membrane-bounded bodies, is also missing in the bacteria-enclosed region. However, cross sections through this part of the axostyle (Fig. 4 a) show that the number of microtubules is the same as in other regions (Fig. 4 b and c). It should also be noted that both layers of the girdle are missing in the axostylar projection, once cells change shape in vitro.

No significant structural differences were observed along the length of the axostyle complex used as the laser target, i.e., from the posterior border of the bacterial bowl to the beginning of the axostylar projection. The number of microtubules remains approximately the same (~400) at all levels (Fig. 4 b and c). The spacing and morphology of the investing microfilaments also do not change from anterior to posterior (Fig. 3). The only morphological difference between anterior and posterior regions of the axostyle involves the spiraling of the sheet of microtubules. Near the posterior end of the cell body, successive coils of the sheet are fairly uniformly spaced (Fig. 4 c). At the anterior end, however, the coils are closer together on one side of the axostyle and farther apart on the opposite side, resulting in a slight increase in the diameter of the rod (Fig. 4 a and b). This eccentricity reflects the asymmetrical origin of the microtubular spiral at the base of the nucleus.

Laser-Induced Breaks in the Axostyle

No breaks could be made at the very anterior end of the axostyle, where the bacteria reside, because wood particles are excluded from this region. The shortest anterior segments obtained (measuring from the Golgi apparatus) thus coincided with the length of the bacteria-enclosed region, i.e., 5–6 μm.

Irradiation caused the target wood particle to swell to an average diameter of 6.0 ± 1.2 μm (n = 88). This granule usually obscured the broken ends of the axostyle, although occasionally one or both ends of the break were visible (Figs. 1 and 7). Regardless of whether or not the broken ends of the axostyle could be seen, an abrupt change in path of the axostyle commonly occurred at the irradiated particle (Fig. 1).

Several observations indicate that the region of axostyle destroyed by the laser beam is considerably smaller than the diameter of the swollen wood particle. In cases where both severed ends were visible, they appeared blunt and cleanly cut with only a very narrow gap separating them (Fig. 7). Length measurements made before and after lasing in these cases (seven cells) revealed a loss of only ~1 μm in length (average). The laser method thus results in a sharply localized break in the axostyle.

Preliminary data indicate that the break can occur at various sites with the ~6 μm region covered by the swollen particle. For this reason, we commonly measured lengths to the boundary of the particle, instead of trying to extrapolate to the true breakpoint.

Immediate Effects of Lasing

Breaking the axostyle resulted in immediate changes in rotation speed of the head and axostylar projection. The effect on head velocity showed a marked dependence on the site of lasing, whereas the effect on the axostylar projection was independent of the level of the break.

AXOSTYLAR PROJECTION: The rotation speed of the axostylar projection always increased about 1.5 times immediately after lasing, and remained constant thereafter (see below).

HEAD ROTATION: SHORT ANTERIOR SEGMENTS: In cells which were lased near the head, and had very short anterior segments $\left(\frac{A_a - A_b}{A - A_b} < 0.15\right)$, the head often stopped turning. The duration of head stoppage was variable and was not related to the length of the anterior

Published July , 1978

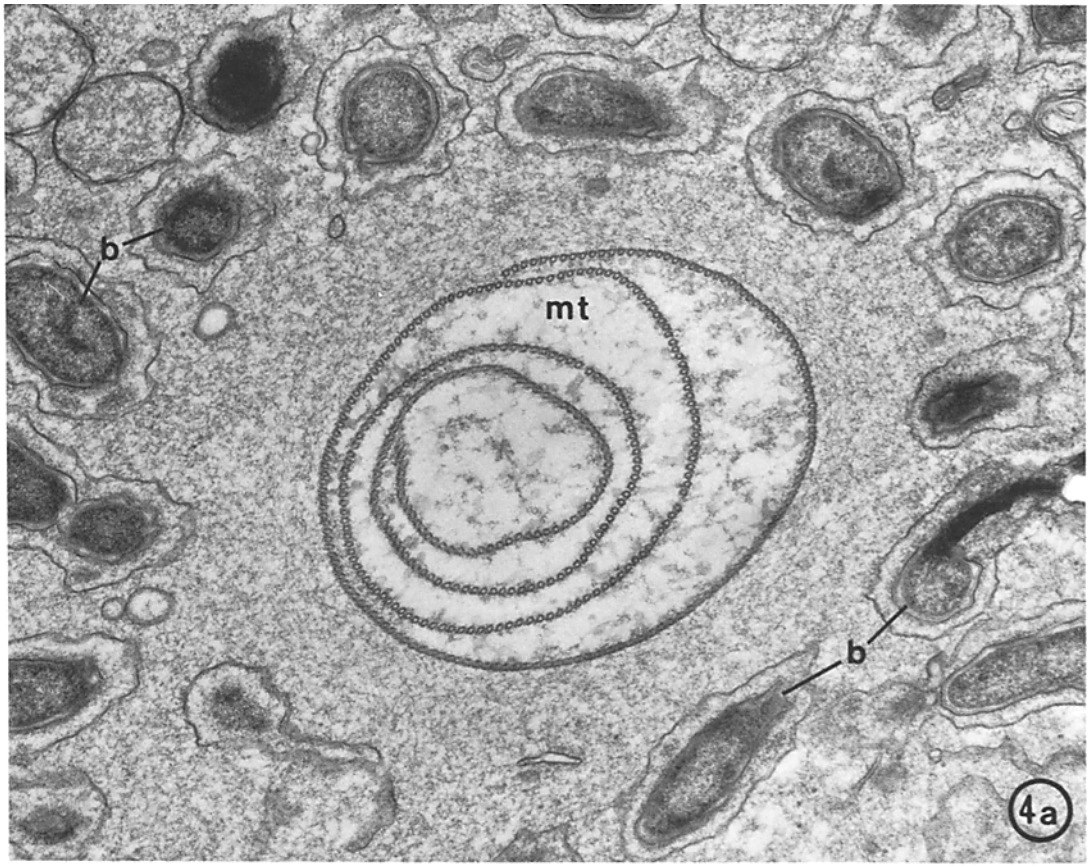

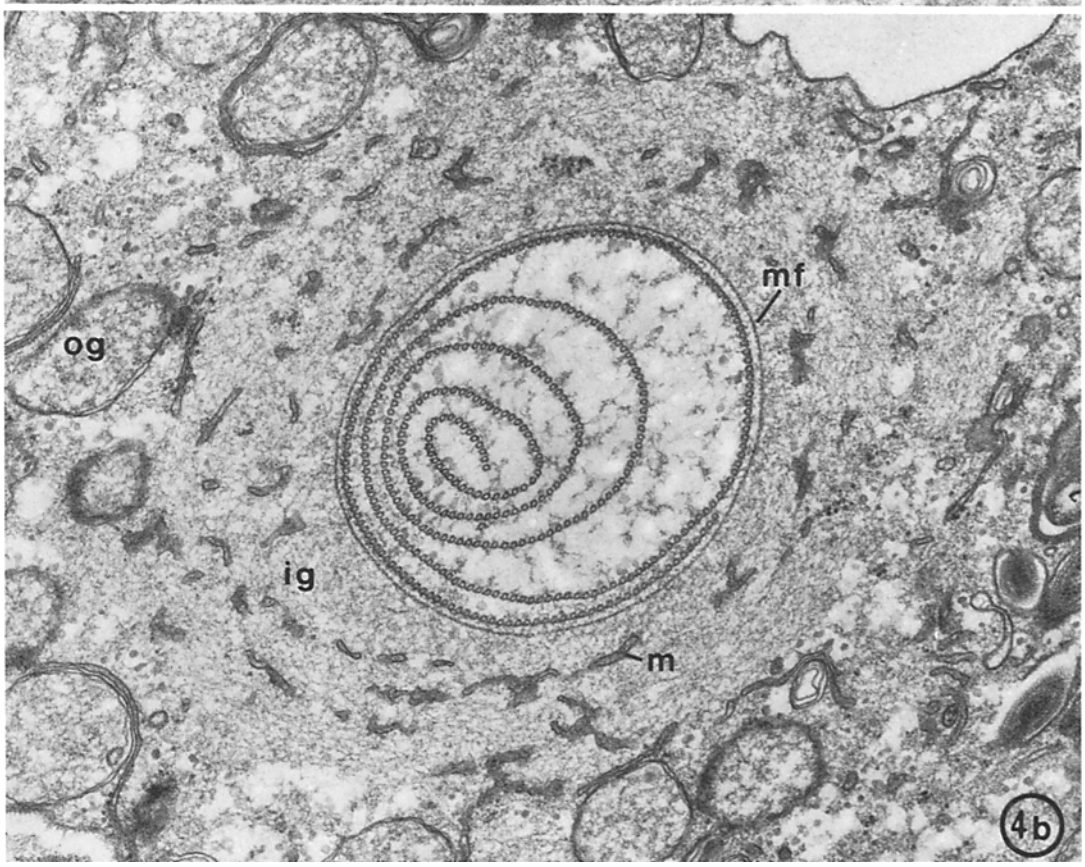

Published July , 1978

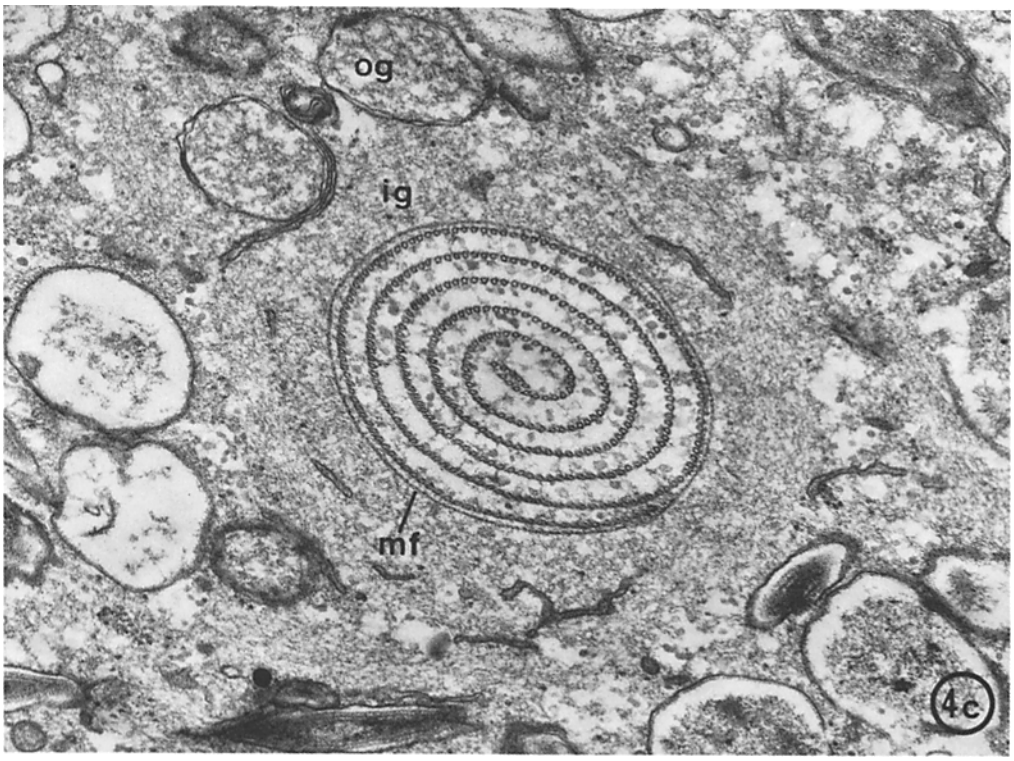

FIGURE 4 Transverse sections through the axostyle complex at different levels in the same cell. (a) anteriormost part surrounded by bowl-shaped group of bacteria (*b*); Fig. 4 b and c, anterior and posterior regions, respectively, corresponding to levels marked in Fig. 1 a. *mt*; microtubular spiral; *mf*, microfilaments; *ig*, inner girdle; *m*, membranous elements of inner girdle; *og*, outer girdle. Sections are viewed from the cell's anterior end (see text). × 35,300.

segment. Some cells showed only an initial pause of several minutes, followed by resumption of head rotation (at speeds described below; cf. Fig. 5); other cells remained stopped for as long as observed (up to 1 h). The latter cases were considered permanently stopped and are plotted as zero velocity in Fig. 6.

The reason for temporary cessation of head rotation is apparently not breakage of the axostyle per se. It was possible to cause the head to stop rotating temporarily by irradiating a particle near the anterior end of the axostyle without actually breaking the axostyle. Such cells resumed head rotation a few minutes later at the same speed as before lasing.

Nor is it likely that cessation of head rotation is due to general "trauma" or nonspecific injury to the cell as a result of lasing its anterior end. In cells showing temporary as well as long-lasting stoppages of head rotation, the posterior segment of the axostyle did not stop turning, but instead speeded up (see above).

Temporary cessation of head rotation thus seems to be a specific type of injury associated with lasing the cell at its anterior end. One possibility is that irradiation near the head induces a temporary gelation at the shear zone, resulting in an increase in resistive torque which blocks head rotation.

The long-lasting stoppage of head rotation in other cells may simply represent a prolonged effect of this injury. On the other hand, irreversible stoppage of head rotation might be a direct result of the short length of the anterior segment, as would be expected if the axostyle complex is the rotary motor.

Cells with short anterior segments also experienced a time-dependent change in rotation speed of the head for a brief period after lasing. Initially, the rotation velocity of the head was extremely

Published July , 1978

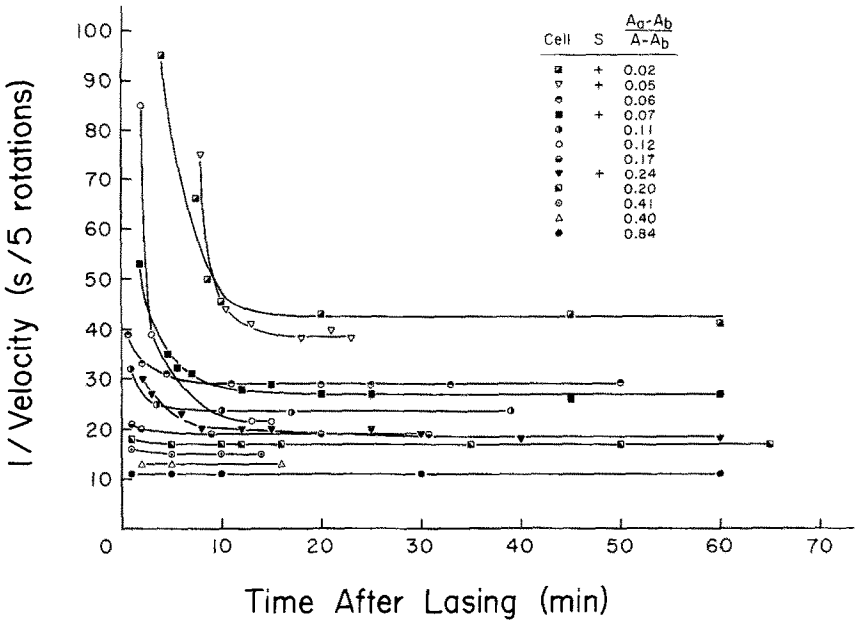

FIGURE 5 Rotation velocity of the head as a function of time after lasing for anterior segments of different lengths. 12 cells with anterior segments ranging from 0.02 to 0.84 relative length ($A_a - A_b/A - A_b$) are shown. t_5 values (inverse of rotation velocity; see Materials and Methods) are plotted directly on the y-axis. Temporary stoppage of head rotation after lasing is denoted by "+" under column *S* of *inset* (see text).

slow; it then increased gradually, until by 10–15 min after irradiation the velocity reached a constant value which was maintained thereafter (Fig. 5). This plateau velocity was always less than the speed before lasing, and was used whenever available for calculating relative velocity (see below).

This time-dependent change in head rotation speed after lasing was most dramatic in cells with the shortest anterior segments, becoming less noticeable at longer lengths (Fig. 5). It always followed cases of temporary cessation of head rotation, and also occurred in many, but not all, cells which showed no initial stoppage. As noted above for lased control cells with unbroken axostyles, head rotation resumed after temporary stoppage without a time-dependent change in speed. Therefore, the initial change in velocity after lasing probably does not represent a stage in recovery from stoppage, or a less severe injury effect. Its cause remains unknown at present.

HEAD ROTATION: LONG ANTERIOR SEGMENTS: Cells with axostyles broken further posteriorly $\left(\frac{A_a - A_b}{A - A_b} > 0.20\right)$ commonly showed neither cessation of head rotation nor time-dependent changes in rotation speed after lasing. Instead, the head usually began rotating at its maximum speed immediately after irradiation (Fig. 5).

Anterior Segment: Head Velocity vs. Length

Fig. 6 shows that rotation speed of the head depends on the length of the anterior segment of axostyle attached to it. At short lengths the velocity of head rotation drops dramatically; but as length of the anterior segment increases, head speed also increases, until the initial velocity before lasing is regained at lengths approaching the original length in the cell body. Velocity does not increase linearly with length; the rate of change in velocity is greatest at short lengths and progressively decreases with increasing length.

The two methods used for determining relative length (Fig. 6a vs. Fig. 6b) differ mainly in the early part of the length-velocity curves. The method which uses the base of the Golgi apparatus as the anterior end of axostyle (Fig. 6a) results in a length-intercept (at zero velocity) of approx. 0.1. This suggests that the anteriormost 10% of

Published July , 1978

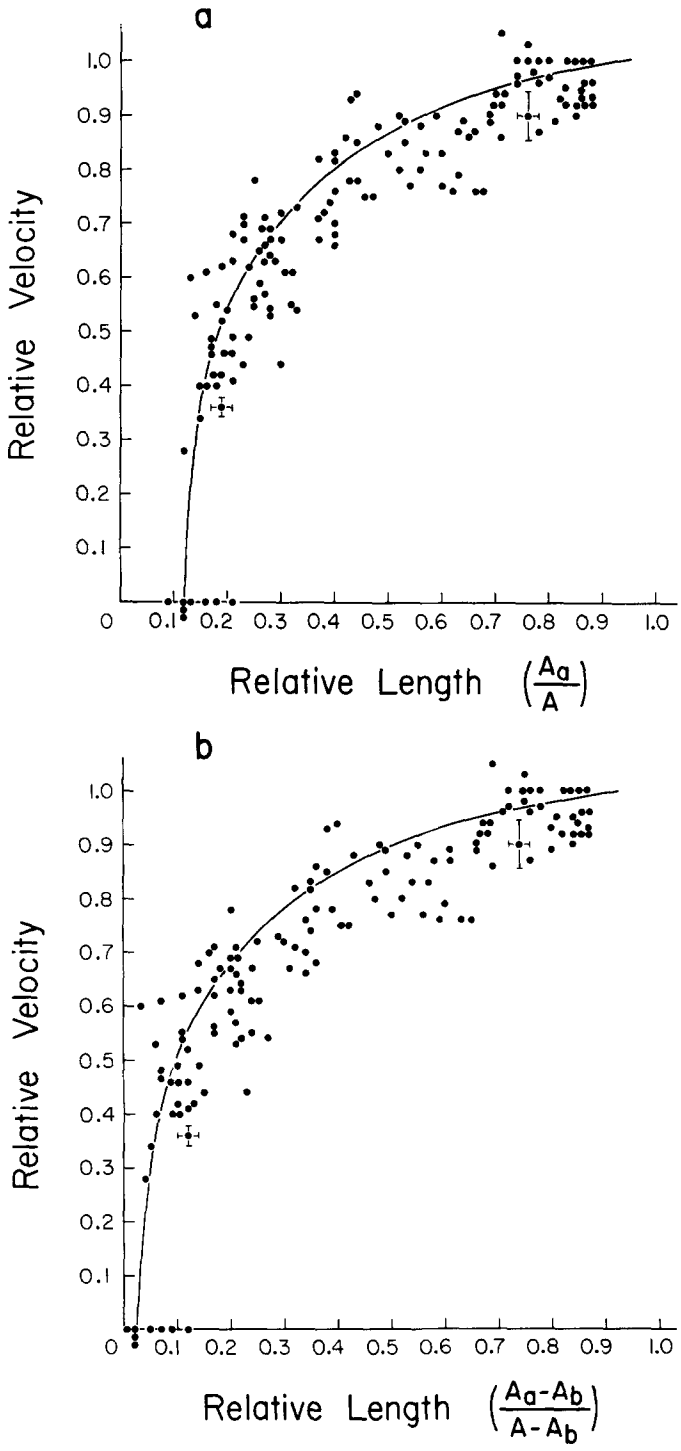

FIGURE 6 Dependence of head rotation velocity on relative length of the anterior segment of axostyle, using the two methods for determining length (see text; Fig. 1).

Curves are drawn by eye. Each point represents one cell. Bars indicate maximum limits of combined errors arising from accuracy of measuring methods and spread of individual values. Length errors due to invisibility of broken ends (cf. Fig. 1 *b*) are not included; their effect would be to displace the entire curves up to 0.1 to the left on the length axis (see Discussion).

Published July , 1978

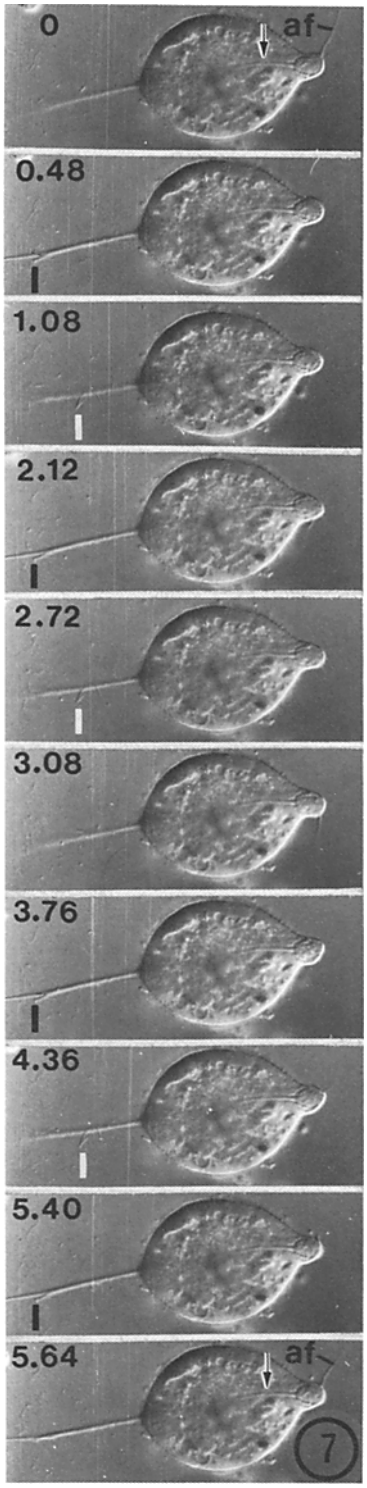

the axostyle cannot by itself cause rotation of the head.

The bacteria-enclosed region at the anterior end of the axostyle also represents about 10% of the length of the axostyle in the cell body. Since the second method for calculating relative length excludes this region from consideration (Fig. 6 b), the length-velocity curve now intercepts the length axis near the origin, i.e., velocity begins increasing almost immediately with length.

Posterior Segment: Axostylar Projection Velocity vs. Length

Unlike that of the head (anterior segment), the rotation speed of the axostylar projection (posterior segment) always increases after lasing. Fig. 8 shows that at any given length the relative velocity of the axostylar projection varies from about 1.2 to 1.8. However, the velocity scatter does not appear to change as a function of length. That the rotation speed of the axostylar projection is indeed independent of the length of the posterior segment was confirmed by a linear regression treatment of the data. Assuming a straight line relationship between length and velocity, the analysis gave a slope of -0.056 ± 0.078 (SD). This is consistent with a slope of zero, i.e., independence of velocity on length, and is indicated in Fig. 8 by a line drawn parallel to the length axis at the mean relative velocity of 1.47.

FIGURE 7 Rotation of head and axostylar projection at different speeds after breaking the axostyle. Before lasing (not shown), both head and axostylar projection rotated at the same velocity (1 rotation/2.60 s). The axostyle was then broken near the anterior end (arrows). This series of prints from a ciné film (time elapsed in s at upper left) shows that the rotation velocity of the head decreased by ~½ after lasing (1 rotation/5.64 s). The papillar insertion of the anterior flagella (*af*) is used to count number of head rotations: one complete rotation occurs between the first and last prints.

In contrast, the rotation velocity of the axostylar projection increased about 1.6 times after lasing (1 rotation/1.64 s). Two sets of filamentous bacteria that adhere to the axostylar projection serve as markers; the time elapsed between successive rotations of each marker to the same position (black and white bars) is 1.64 s.

Both severed ends of the axostyle are visible (arrows), and appear cleanly cut with only a narrow gap between them. 25 fps, Kodak Plus-X film. (Reprinted with permission from Tamm [17]).

Published July , 1978

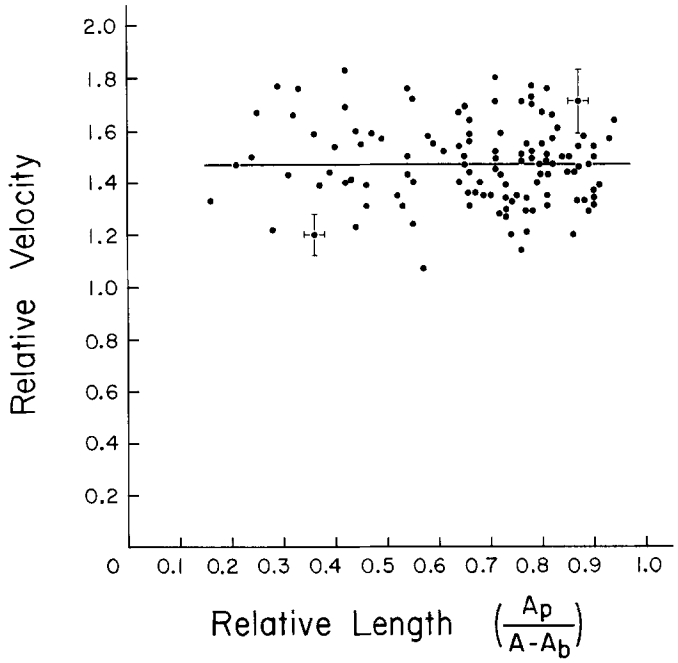

FIGURE 8 Independence of rotation speed of the axostylar projection on relative length of the posterior segment of axostyle. Horizontal line at the mean relative velocity (1.47) was fitted to the data by linear regression (see Results). Error limits have the same meaning as in Fig. 6. Each point represents one cell.

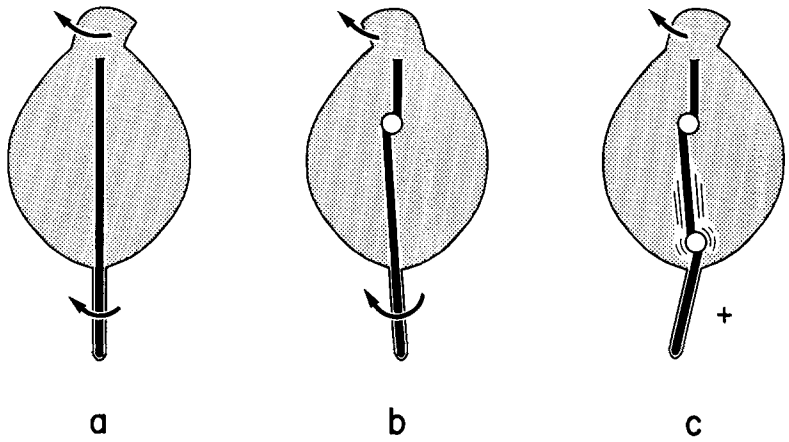

FIGURE 9 Rotation of a third segment of axostyle, independent of the head and axostylar projection. Before lasing (a), head and axostylar projection rotated at the same speed (curved arrows). After breaking the axostyle near the anterior end (b), the rotation speed of the head decreased, while that of the axostylar projection increased. A second break made close to the axostylar projection created a third, middle segment (c). The axostylar projection then stopped turning, while the middle segment (and lased wood particle at the second break site) oscillated at a frequency greater than that of head rotation (see text).

Published July , 1978

When the axostyle is broken at the posterior end of the cell body, the axostylar projection always stops turning (cf. Fig. 9 c).

Rotation of a Third, Middle Segment of the Axostyle

In one experiment the axostyle was first broken a short distance from the anterior end (see Fig. 9). As expected, the rotation speed of the head decreased, while that of the axostylar projection increased. A second break was then made in the posterior segment, close to the beginning of the axostylar projection. This created a third segment, not connected to the head or axostylar projection (Fig. 9 c). After the second dissection, the axostylar projection stopped rotating. The middle segment and the lased particle at the second break wobbled periodically at a frequency greater than that of head rotation. Taking this oscillation as a sign of rotation, these results show that a segment of the axostyle which is physically isolated from the head and axostylar projection can rotate by itself.

Electric Model of the Axostylar Rotary Motor

Simulated laser experiments were performed on an electric model of the axostyle (Fig. 10).

Comparison of the length-velocity curves for the model (Fig. 11) and the cells (Figs. 6 and 8) shows that the model behaves like the cells. For example, rotation speed of the model's head increases with the number of motors connected to it, i.e., axostyle length. Head velocity is not a linear function of the number of motors, however, but is maximal at first, and then slows down as additional motors are added. This relationship resembles the length-velocity curve for the anterior segment of lased cells (Fig. 6).

The rotation speed of the model's axostylar projection remains equal to that of the free-running motors, i.e., 2,500 rpm, regardless of the number of motors driving it (Fig. 11). The same independence of rotation velocity on length of the posterior segment was found in actual experiments (Fig. 8).

DISCUSSION

The laser experiments provide direct evidence that the axostyle complex generates the torque for rotational motility in a devescovinid flagellate. By demonstrating rotation of anterior and posterior segments of the axostyle regardless of the level of break, the present study also confirms indirect evidence (16) that the torque-generating mechanism is distributed along the length of the axostyle complex. A possible exception is the bacteria-enclosed part of the axostyle at the anterior end (see below). Although the distal part of the axostyle probably generates torque before the cells change shape in vitro, once this part becomes the axostylar projection, it can not be providing any torque. Not only does the entire axostylar projection turn, but breaks near the axostylar projection cause it to stop rotating and do not result in a decrease in rotation speed of the head. The head and axostylar projection are therefore turned by the proximal part of the axostyle within the cell body.

The dependence of head rotation velocity on length of the anterior segment (Fig. 6) indicates that the head offers a resistive torque, i.e., the head is a load on the rotary motor. The torque supplied by the anterior segment increases with its length, since the force-generating machinery is distributed along the axostyle. The resistive torque of the head is also evident from the increase in rotation speed of the axostylar projection after severing the posterior part of the axostyle from the head. Experiments are now underway to determine the relative contributions of external viscous drag and internal cytoplasmic resistance in the shear zone to the net resistive torque of the head.

In contrast to the head, the resistive torque offered by the axostylar projection must be negligible, since its rotation velocity is independent of the length of the posterior segment, and the rotation speed of the head never increases after breaking the axostyle near the posterior end of the cell body.

Structure-Function Relations

The finding that the bacteria-enclosed part of the axostyle can not, by itself, turn the head may be due to inability of this region to generate torque. Alternatively, the bacteria-enclosed region may be active, but not long enough to overcome the resistive torque of the head, i.e., subthreshold length.

In view of the structural deficiencies found in this part of the axostyle complex (Figs. 2 and 4), these possibilities have important implications for identifying elements of the rotary motor. Inactiv-

Published July , 1978

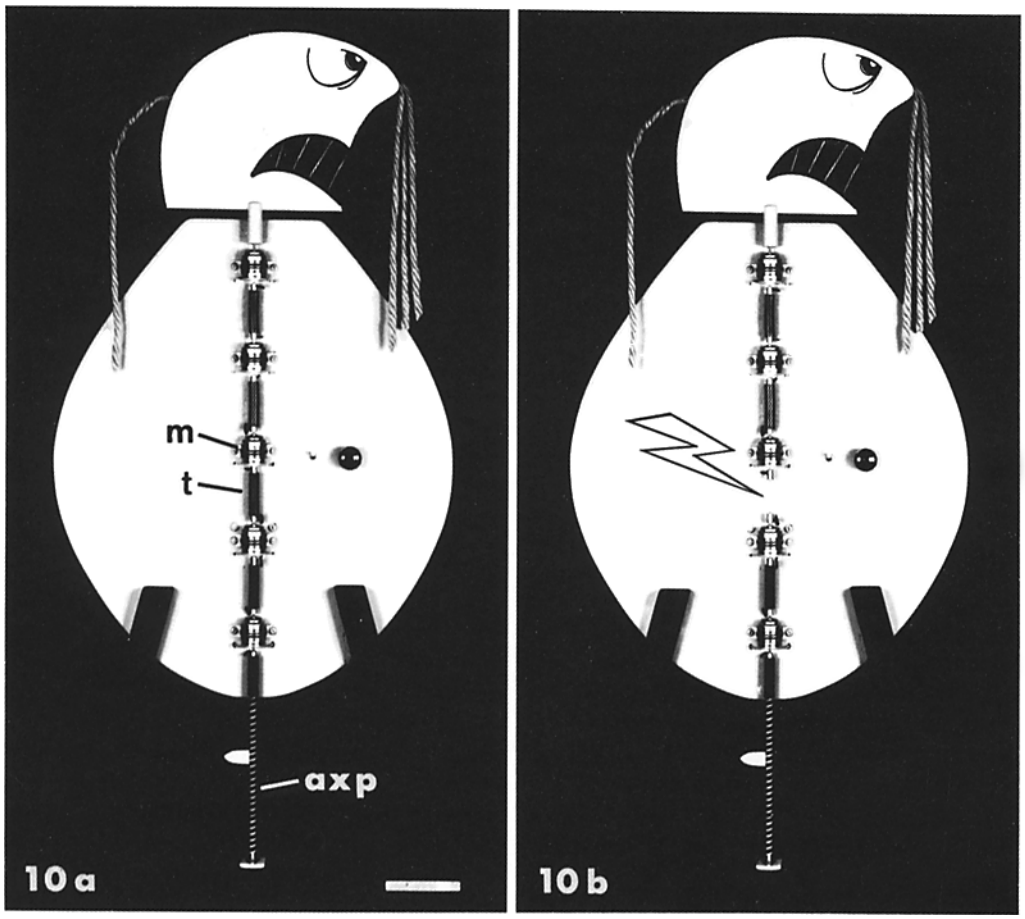

FIGURE 10 Electric model of axostylar rotary motor before (a) and after (b) "lasing." Five double-shafted DC motors (*m*) in series represent the axostyle in the cell body. The motors are electrically independent and are calibrated to the same free-running speed (2,500 rpm). Adjacent motors are mechanically coupled by pieces of rubber tubing (*t*). The anteriormost motor is connected to a flat cardboard "head;" the posteriormost motor is connected to the "axostylar projection" (*axp*), a striped rod with a velocity marker, resting in an almost frictionless Teflon bearing.

Laser-induced dissection of the axostyle at a given level is simulated by removing the appropriate piece of tubing between adjacent motors (laserbolt in Fig. 10b). Rotation velocities of head and axostylar projection were measured as functions of number of motors, i.e., segment length; cf. Fig. 11. Bar, 7 cm. inches.

ity of the bacteria-enclosed region would support our previous idea (15) that extra-microtubular components, i.e., inner girdle and microfilaments, are the real motor, whereas the second possibility argues strongly for an active role of the microtubules themselves.

We cannot decide between these alternatives at present. However, it should be noted that an active but subthreshold length of the axostyle could still exist even if the bacteria-enclosed region were unable to generate torque. This is because segment lengths were commonly measured to the apparent broken ends at the edges of the irradiated particle (average diameter = 6 μm). The measured lengths thus represent minimum values; actual lengths may be up to 10% longer. Thus, the length intercept in Fig. 6b may really be closer to 0.1 than to the origin, leaving room for a subthreshold length posterior to the bacteria-enclosed region.

Published July , 1978

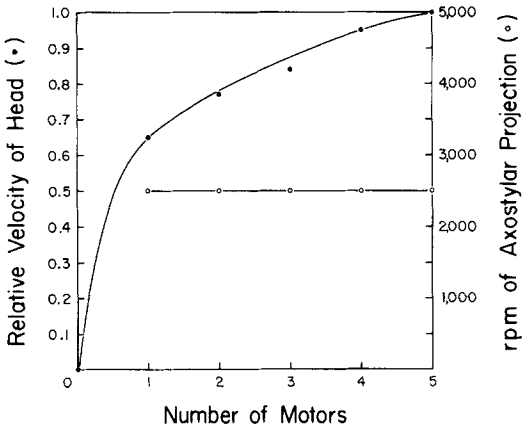

FIGURE 11 Length-velocity relationships for anterior and posterior segments of the electric model (cf. Fig. 10). Rotation speed of the head is expressed relative to speed before "lasing," while rotation speed of the axostylar projection is given in absolute rpm's. The number of motors driving the head or axostylar projection, multiplied by 0.20, corresponds to the relative length of the anterior or posterior segment.

Length-Velocity Relationships: Anterior Segment

One possible reason for the nonlinearity of the length-velocity curve for the anterior segment (Fig. 6) is that the force generated per unit length of the axostyle varies along the length, being greater near the anterior end. Alternatively, torque per unit length may be constant, but other factors may make the curve nonlinear.

Several lines of evidence argue against the former explanation and for the latter. We could find no significant structural differences in the axostyle complex along its length (excluding, of course, the bacteria-enclosed part). Nevertheless, antero-posterior differences in unrecognized structures, or rate-limiting molecules (enzymes, energy source), cannot be ruled out.

The electric model of the axostyle shows how a nonlinear length-velocity curve can be obtained with constant force production per unit length, i.e., per motor. In this case, the shape of the curve is due to the relation between resistive torque of the model's head and its angular velocity (where external drag $\propto$ velocity^2), and to the relation between angular velocity and torque for motors in series where torques are summed (D. Novotny, University of Wisconsin, personal communication).

Several discrepancies obviously exist between the model and the cells. The model operates at high Reynolds number, whereas viscous forces are more important than inertial ones for the protozoa. Also, the resistive torque of the model's head is due solely to external drag, but the devescovinids must experience internal cytoplasmic resistance as well. Therefore, the close similarity between the length-velocity curves for the anterior segments of the model and the cells is probably coincidental.

Nevertheless, the differences between the two systems are not crucial to the explanatory value of the model. For example, velocity-torque diagrams for the model show that the slope of its length-velocity curve still declines with length even when external drag is assumed to be a linear function of angular velocity (as would be the case for a rotating hemispherical surface at low Reynolds number, i.e., the head of the cells). The important point is that the model suggests a simple way to explain the nonlinear nature of the length-velocity curve without having to assume any differences in force production per unit length along the axostyle. The same kind of explanation may well account for the behavior of the anterior segment in actual cells, once the resistive effects of the head are understood.

Length-Velocity Relationships: Posterior Segment

The rotation speed of the model's axostylar projection is independent of the number of motors turning it, because the axostylar projection offers essentially no resistive torque, and each motor has the same angular velocity at zero external load. Rotation velocity depends solely on the free-running speed of the motors themselves. The similar length-velocity relationship found for the posterior segment of lased cells can be explained in the same way. Thus, the rotation speed of the posterior segment, as indicated by the axostylar projection, represents the speed of the free-running axostylar motor, i.e., under conditions of essentially no load.

CONCLUSION

This study has identified the axostyle complex as the rotary motor responsible for a remarkable kind of cell motility, and characterized several of its dynamic properties. The major question remains, however: How does the axostyle complex generate torque?

Published July , 1978

Many kinds of nonmuscle cell motility are believed to work by active shearing between actin and myosin filaments, or between microtubules and dynein (5, 7, 10–14). In both cases, ATP-powered cross-bridges are thought to provide the motive force for sliding. However, exceptional types of cell motility which do not operate by such a mechanism apparently exist (1–3, 6, 9). The question can therefore be asked: Does the axostylar rotary motor work by a cross-bridge driven shearing interaction between some of its components, or is it another exception to this scheme?

At present, consideration of this question must rely almost exclusively on what is known about the structure of the axostyle complex. The presence of both microtubules and microfilaments in the axostyle provides at least some of the components required for models based on sliding. The microtubules, however, run perpendicular to the direction that force must be exerted to turn the axostyle. Therefore, sliding between microtubules seems an unlikely mechanism for causing rotational movements. The microfilaments, on the other hand, run parallel to the expected direction of force production, suggesting that they may be part of the rotary motor. The possible role of the microfilaments in generating torque, and the applicability of an actin-myosin shearing mechanism to this motility are now under investigation.

It is a pleasure to thank Professor T. M. Sonneborn, Indiana University, for generously providing an argon laser for this study. I am grateful to Dr. Gary Borisy and the Laboratory of Molecular Biology and Biophysics, University of Wisconsin, for use of electron microscopy facilities, secretarial help, and general lab support. Dr. Peter Luykx and Mr. Robert Syren, University of Miami, have continued to given enthusiastic assistance in collecting *Cryptotermes cavifrons*. I also thank Dr. Donald Novotny, Electrical Engineering, University of Wisconsin; Dr. Howard Winet, Southern Illinois University; Dr. Charles Brokaw, California Institute of Technology; and Dr. Stuart Keller, Columbia University, for stimulating discussions of the data. Dr. Robert Scheele, University of Wisconsin, performed the linear regression analysis by computer, and Dr. Carol Allen, University of Wisconsin, read and critized several versions of the manuscript.

This work was supported by National Science Foundation grant PCM76-01943.

Received for publication 18 November 1977, and in revised form 22 February 1978.

Note Added in Proof: Flattening cells in the presence of polyene antibiotics (50 μM amphotericin B or nystatin) often allows reactive torque to be expressed. In these cases, clockwise rotation of the head and axostyle is prevented, but cytoplasmic particles lying close to the axostyle rotate counterclockwise around it. Rotation speed of the particles does not vary significantly from anterior to posterior along the axostyle. The bowl-shaped group of bacteria surrounding the anterior part of the axostyle never rotates, even though particles immediately behind it turn. These findings confirm that force production per unit length is constant along the length of the axostyle, and they indicate that the bacteria-enclosed region does not generate torque. Thus, the electric model's explanation of the length-velocity curve for the anterior segment is supported, and the postulated role of microfilaments in rotational motility is strengthened.

REFERENCES

1. Amos, W. B. 1975. Contraction and calcium binding in the vorticellid ciliates. *In* Molecules and Cell Movement. S. Inoué and R. E. Stephens, editors. Raven Press, New York. 411–436.
2. Berg, H. 1974. Dynamic properties of bacterial flagellar motors. *Nature (Lond.)*. **249:**77–79.
3. Berg, H. 1975. Bacterial behaviour. *Nature (Lond.)*. **254:**389–392.
4. Berns, M. W. 1974. Recent progress with laser microbeams. *Int. Rev. Cytol.* **39:**383–411. Academic Press, Inc., New York.
5. Bloodgood, R. A. 1975. Biochemical analysis of axostyle motility. *Cytobios.* **14:**101–120.
6. Cachon, J., Cachon, L. G. Tilney, and M. S. Tilney. 1977. Movement generated by interactions between the dense material at the ends of microtubules and non-actin-containing microfilaments in *Sticholonche zanclea*. *J. Cell Biol.* **72:**314–338.
7. Goldman, R., T. Pollard, and J. Rosenbaum. 1976. Cell Motility. *Cold Spring Conf. Cell Proliferation.* **3:**1–1373.
8. Kirby, H. 1949. Devescovinid flagellates of termites. V. The genus *Hyperdevescovina,* the genus *Bullanympha*, and undescribed or unrecorded species. *Univ. Calif. Publ. Zool.* **45:**319–422.
9. Larsen, S. H., J. Adler, J. J. Gargus, and R. W. Hogg. 1974. Chemomechanical coupling without ATP: the source of energy for motility and chemotaxis in bacteria. *Proc. Natl. Acad. Sci. U. S. A.* **71:**1239–1243.
10. Mooseker, M. S., and L. G. Tilney. 1973. Isolation and reactivation of the axostyle. Evidence for a dynein-like ATPase in the axostyle. *J. Cell Biol.* **56:**13–26.
11. Pollard, T. D., and R. R. Weihing. 1974. Actin and myosin and cell movement. *CRC Crit. Rev. Biochem.* **2:**1–65.
12. Sale, W. S., and P. Satir. 1977. Direction of active sliding of microtubules in *Tetrahymena* cilia.

Proc. Natl. Acad. Sci. U. S. A. **74:**2045–2049.

13. SATIR, P. 1974. The present status of the sliding microtubule model of ciliary motion. *In* Cilia and Flagella. M. A. Sleigh, editor. Academic Press, Inc., New York. 131–142.
14. SUMMERS, K. E., and I. R. GIBBONS. 1971. Adenosine triphosphate-induced sliding of tubules in trypsin-treated flagella of sea urchin sperm. *Proc. Natl. Acad. Sci. U. S. A.* **68:**3092–3096.
15. TAMM, S. L. 1976. Properties of a rotary motor in eukaryotic cells. Cell Motility. *Cold Spring Harbor Conf. Cell Proliferation.* **3:**949–967.
16. TAMM, S. L., and S. TAMM. 1974. Direct evidence for fluid membranes. *Proc. Natl. Acad. Sci. U. S. A.* **71:**4589–4593.
17. TAMM, S. L., and S. TAMM. 1976. Rotary movements and fluid membranes in termite flagellates. *J. Cell Sci.* **20:**619–639.